

Quantitative Assessment of Regional Alveolar Ventilation and Gas Volume Using $^{13}\text{N-N}_2$ Washout and PET

Jean-Christophe Richard, MD, PhD^{1,2}; Marc Janier, MD, PhD^{3,4}; Franck Lavenne³; Christian Tourvieille³; Didier Le Bars, PharmD, PhD³; Nicolas Costes³; Gerard Gimenez, PhD³; and Claude Guerin, MD, PhD^{1,2}

¹Service de Réanimation Médicale et d'Assistance Respiratoire, Lyon, France; ²Equipe d'Accueil Universitaire, Lyon, France; ³Hôpital Neuro-Cardiologique, Centre d'Exploration et de Recherche Médicales par Émission de Positons, Lyon, France; and ⁴Hôpital Neuro-Cardiologique, Centre de Recherche et d'Application en Traitement de l'Image et du Signal (Unité Mixte de Recherche, Centre National de la Recherche Scientifique), Batiment Centre d'Etudes et de Recherche Médicales par Émission de Positons, Lyon, France

Measurement of alveolar volume (V_A) and regional ventilation (\dot{V}_A) is crucial to understanding the pathophysiology of acute lung injury and ventilator-induced lung injury. PET has previously been used as a noninvasive, quantitative method to assess \dot{V}_A , but formal validation of this technique in experimental lung injury is lacking. This study aims to validate V_A and \dot{V}_A regional assessment with PET, using inhaled $^{13}\text{N-N}_2$ in pigs.

Methods: Two normal and 2 oleic acid-injured pigs were tracheotomized, mechanically ventilated, and studied in 5 different levels of ventilation by changing respiratory rate. In each experimental condition, lungs were washed-in and then washed-out with $^{13}\text{N-N}_2$ through an open circuit in the ventilator. Using this method, multiframe images were acquired with a dedicated PET camera. Regions of interest (ROIs) were drawn on each lung. Regional time-activity curves during washout were generated for each ROI and fitted to a mono- and a bi-compartmental model. Validation of this method was performed in 2 ways. First, regional values of predicted V_A ($V_{A\text{emission}}$) were compared with regional volume obtained independently from density analysis on a transmission scan ($V_{A\text{trans}}$). Second, regional values of predicted \dot{V}_A were summed in each animal during each experimental condition and compared with minute-ventilation values set on the ventilator. **Results:** The bi-compartmental model best fitted the experimental values in normal (94.7% [62.2%–100.0%]) (median [interquartile range]) of the ROIs as well as in injured animals (90.7% [81.6%–97.4%]) of the ROIs ($P = 0.49$). $V_{A\text{emission}}$ significantly correlated with $V_{A\text{trans}}$ ($R^2 = 0.89$, $P < 0.001$) but exceeded $V_{A\text{trans}}$ by 10%. Finally, \dot{V}_A strongly and positively correlated with minute-ventilation in both normal ($R^2 = 0.96$, $P < 0.001$) and injured ($R^2 = 0.96$, $P < 0.001$) animals. **Conclusion:** Measurement of $^{13}\text{N-N}_2$ washout using PET is accurate to assess regional alveolar volume and ventilation during experimental acute lung injury.

Key Words: PET; ventilation; ^{13}N ; oleic acid; lung injury

J Nucl Med 2005; 46:1375–1383

Ventilator-induced lung injury (VILI) during mechanical ventilation of injured lungs has been clearly recognized for many years. VILI may result from overdistension of the most anterior lung regions (1) or from repeated small airways opening and closing in the most dependent parts of the lungs (2). Preventing VILI is a major goal when mechanically ventilating patients with acute lung injury (ALI) because reduction of lung overdistension can affect patient outcome (3). Assessment of the distribution of lung ventilation is therefore crucial for better use of the ventilatory support. The field of lung imaging is expanding dramatically by providing several new techniques or refinement of older ones, such as SPECT (4), xenon-enhanced CT (5), MRI (6), and synchrotron radiation CT (7). However, PET is a powerful, noninvasive technique to measure tissue concentration of physiologic tracers. PET has already been used to study regional lung ventilation using a short-lived positron emitter, $^{13}\text{N-N}_2$ (half-life [$t_{1/2}$] = 9.96 min), infused into the blood (8–10) or injected into a closed rebreathing circuit (11). We report a new simple quantitative method using PET and $^{13}\text{N-N}_2$ inhalation in an open circuit. We address the theoretic background of lung ventilation measurement as derived from tracer kinetics modeling during washout and present a formal validation in vivo.

MATERIALS AND METHODS

Animal Preparation

This study was performed on 4 female pigs (mean weight \pm SD, 32 ± 2 kg). They were premedicated with an intramuscular injection of xylazine (20 mg), ketamine (500 mg), and droperidol (10 mg), then anesthetized with 100 mg intravenous propofol, followed by a continuous intravenous infusion of 350 mg/h. Analgesia was performed with continuous intravenous infusion of fentanyl (0.1 mg/h). Muscle relaxation was obtained with continuous intravenous infusion of pancuronium bromide (3 mg/h).

After tracheotomy, all pigs were mechanically ventilated in supine position, using a volume-controlled mode with a squared inflation flow (Cesar II ventilator; Taema): fraction of inspired

Received Dec. 2, 2004; revision accepted Apr. 19, 2005.
For correspondence or reprints contact: Claude Guerin, MD, PhD, Service de Réanimation Médicale et d'Assistance Respiratoire, 103 Grande Rue de la Croix-Rousse, Lyon 69004, France.
E-mail: claude.guerin@chu-lyon.fr

oxygen (F_{IO_2}), 21%; tidal volume (V_T), 10 mL/kg; and respiratory rate, 20 breaths/min on zero end-expiratory pressure. F_{IO_2} was set to 100% at the end of animal preparation.

Experimental Protocol

Animals were randomly assigned to a control group (2 animals) and a lung injury group (2 animals). Lung injury was performed using 0.12 mL/kg of oleic acid (OA) injected intravenously over 20 min. If necessary, additional injections of 0.02 mL/kg OA were repeated until a P_{O_2}/F_{IO_2} ratio of <300 was obtained (12). To achieve stable pulmonary injury, a 110-min period was allowed after OA injection (13).

Animals were studied at 5 levels of minute-ventilation (expired volume per unit time, \dot{V}_E) by changing respiratory rate. A \dot{V}_E of 2, 4, 6, 8, and 10 L/min was applied in control animals and of 4, 6, 8, 10, and 12 L/min in injured animals, on a random basis. Therefore, investigating a large range of regional ventilation was expected.

$^{13}\text{N-N}_2$ Administration

$^{13}\text{N-N}_2$ was continuously generated by a cyclotron using a nitrogen gas target (14) and flushed into an infusion line at a rate of 150 mL/min by a mass flow-meter, yielding a specific activity of 4.2 ± 0.3 MBq/mL at the entry of the ventilator (Fig. 1). A 10-mL loop of this line, inserted inside a dose calibrator, allowed continuous monitoring of $^{13}\text{N-N}_2$ input radioactivity. To guarantee a constant concentration of tracer during the respiratory cycle, administration of $^{13}\text{N-N}_2$ into the inspiratory limb of the respiratory circuit was performed synchronously with the ventilator inspiratory valve opening, using the following procedure (Fig. 1). Airflow analogic output was sent from the ventilator to a data acquisition unit (MP100; Biopac Systems Inc.) connected to a laptop computer, and sampled at 200 Hz. A digital signal was generated (Acknowledge software; Biopac Systems Inc.) to drive

an electric valve located at the $^{13}\text{N-N}_2$ infusion line. $^{13}\text{N-N}_2$ was then diverted to either inspiratory limb of the ventilator during inspiration or to waste container during expiration.

PET Studies

PET studies were performed using an ECAT EXACT HR+ 3-dimensional PET scanner (Siemens) (15). Roughly 15 cm were scanned from lung apex to 2–3 cm below the diaphragm dome, and the animal position within the field of view was controlled by reconstruction of transmission scans. Transmission scans were also performed to correct subsequent emission data for attenuation and to assess pulmonary density and alveolar gas volume (V_A).

Lungs were washed-in with $^{13}\text{N-N}_2$ for 10 min, using inspiratory synchronization, yielding to an approximate dose of 1,900 MBq effectively delivered to the animal lungs. In preliminary experiments, 10 min was found to be sufficient to obtain regional equilibrium within the lungs in control and OA animals. At this time, tracer concentration in the airways is constant over the respiratory cycle. A 5-mL gas sample was drawn at the Y piece level over 1 min using an automated withdrawal pump (Fig. 1), and its specific activity was measured in a well counter. Counts were corrected for physical decay to the time of sampling and expressed as becquerels per milliliter (Bq/mL) of gas. This value represents tracer input function into the lungs and is referred to as C_{INPUT} . To ensure perfect agreement between well counter and PET measurements, a cross-calibration between the 2 devices was realized.

Once activity reached a plateau, $^{13}\text{N-N}_2$ inhalation was stopped and PET emission images were performed serially for 4 min (Fig. 2) to obtain washout curves of tracer, as follows: 12 images of 5-s duration each, 3 images of 20-s, and 2 images of 60-s.

Then, 370 MBq of H_2^{15}O were injected intravenously in 60 s and image acquisition was performed over 6 min, starting 4 min

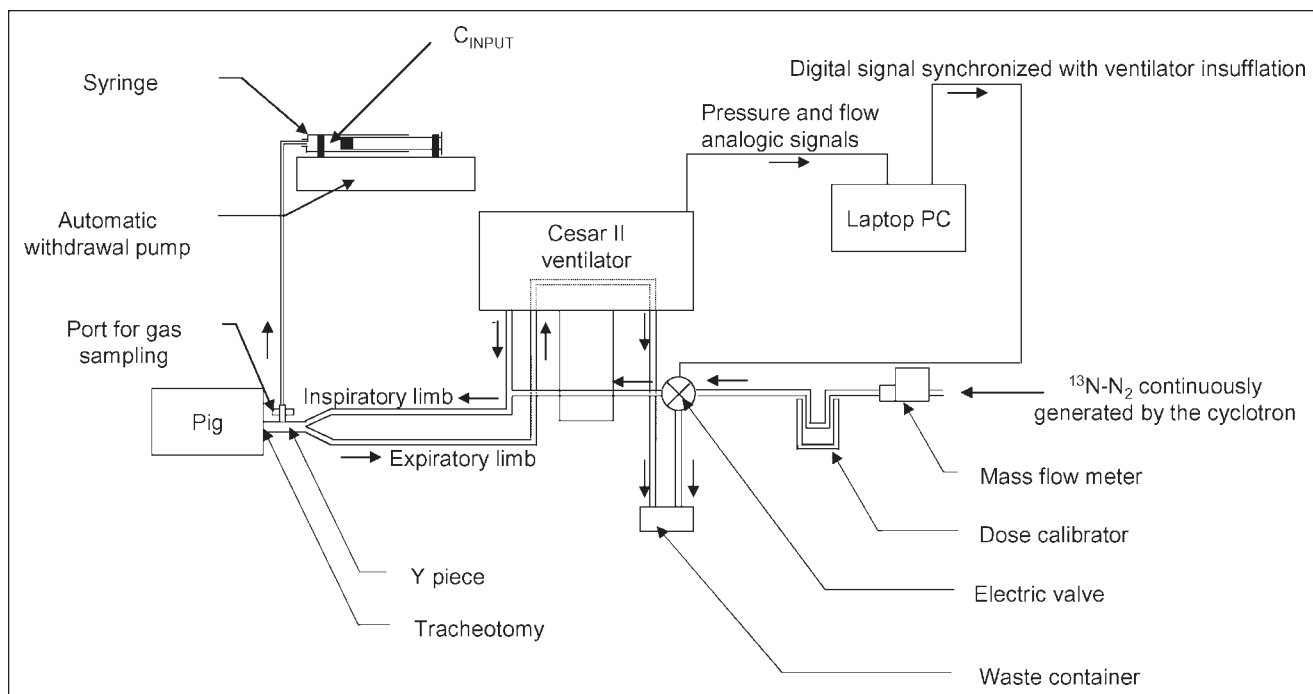


FIGURE 1. Experimental setup to deliver $^{13}\text{N-N}_2$ to lungs. C_{INPUT} is tracer concentration measured at equilibrium at the Y piece level.

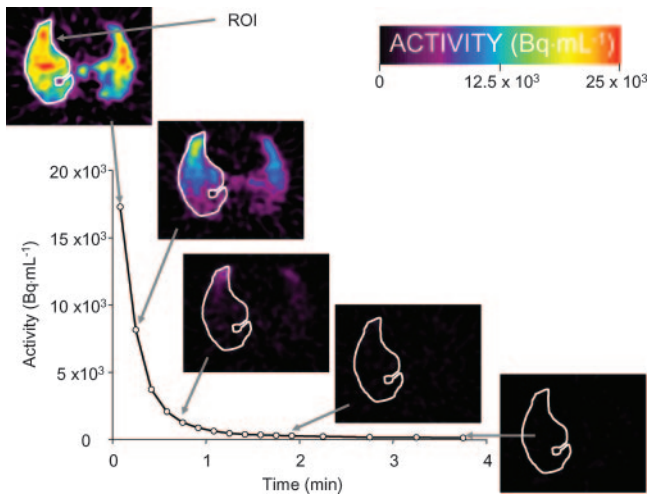


FIGURE 2. Generation of a pulmonary time-activity curve from the multiple-image dataset during washout in 1 pig. Regions of interest (ROIs) are drawn on multiple transverse slices of the first PET image obtained during washout (0–5 s) of $^{13}\text{N-N}_2$. These ROIs are then superimposed on subsequent frames. For clarity, only one ROI and one of the multiple thoracic slices are displayed on 5 of 37 time points.

after tracer injection (H_2^{15}O equilibrium scans). This was done to better delineate the regions of interest (ROIs) in the lungs.

Image Analysis

After image reconstruction for each scan, 63 transversal planes were obtained and summed by 3, resulting in 21 planes used for image analysis. Planes 1 and 21 were excluded because camera detection is not accurate in these peripheral planes. ROIs were drawn on both lungs using transmission scans and superimposed to H_2^{15}O equilibrium scans (16). ROIs were subsequently refined to include poorly ventilated lung areas that were undetected on transmission scans in injured animals but much easier seen on H_2^{15}O images because of the high water content (17). ROIs were then superimposed on $^{13}\text{N-N}_2$ scans to obtain a measurement of pulmonary radioactivity, decay corrected back to the beginning of iso-

tope washout. Finally, lung time-activity curves were generated from the multiple-image dataset (Fig. 2).

Data Analysis

Density Analysis on Transmission Scans. Alveolar gas volume was determined on transmission scans ($V_{A\text{trans}}$) based on the close correlation between photon attenuation and physical density. Calibration of the PET device was performed during transmission scans on phantoms of known density, giving a calibration factor for converting PET attenuation into a quantitative measure of density (18). Regional thoracic attenuation assessed on transmission scans was then converted into regional density (Fig. 3). For each ROI, $V_{A\text{trans}}$ was then determined as follows:

$$V_{A\text{trans}} = (1 - ROI_{\text{density}}) \times ROI_{\text{volume}},$$

$$V_{A\text{trans}} = 0, \text{ if ROI density} \geq 1 \text{ g/mL.} \quad \text{Eq. 1}$$

Tracer Kinetic Models. To describe pulmonary $^{13}\text{N-N}_2$ kinetics, a monocompartmental model and a bicompartamental model were investigated. The former reduced $^{13}\text{N-N}_2$ kinetics to a single alveolar compartment. The bicompartamental model attempted to account for intraregional heterogeneity in ventilation and was constructed by subdividing the aerated compartment into a fast and a slow compartment working in parallel.

General Assumptions. There are 4 basic assumptions subtending our modeling: (i) tidal ventilation can be adequately represented by unidirectional flow with a constant alveolar volume, (ii) removal of tracer by pulmonary blood is negligible, (iii) ventilation and alveolar gas volume remain constant during washout, and (iv) tracer fully equilibrates in alveolar gas.

Monocompartmental Model. From tracer mass equation within alveolar space, the net rate of change of tracer concentration is written as follows:

$$V_A \frac{dC_A(t)}{dt} = \dot{V}_A \times C_I(t) - \dot{V}_A \times C_A(t) - \dot{Q} \times C_V(t) + \dot{Q} \times C_{PA}(t),$$

Eq. 2

where V_A is alveolar gas volume, $C_A(t)$ is $^{13}\text{N-N}_2$ alveolar concentration, $C_I(t)$ is $^{13}\text{N-N}_2$ concentration in inhaled gas, \dot{V}_A is alveolar ventilation, \dot{Q} is pulmonary perfusion, $C_V(t)$ is $^{13}\text{N-N}_2$ concentra-

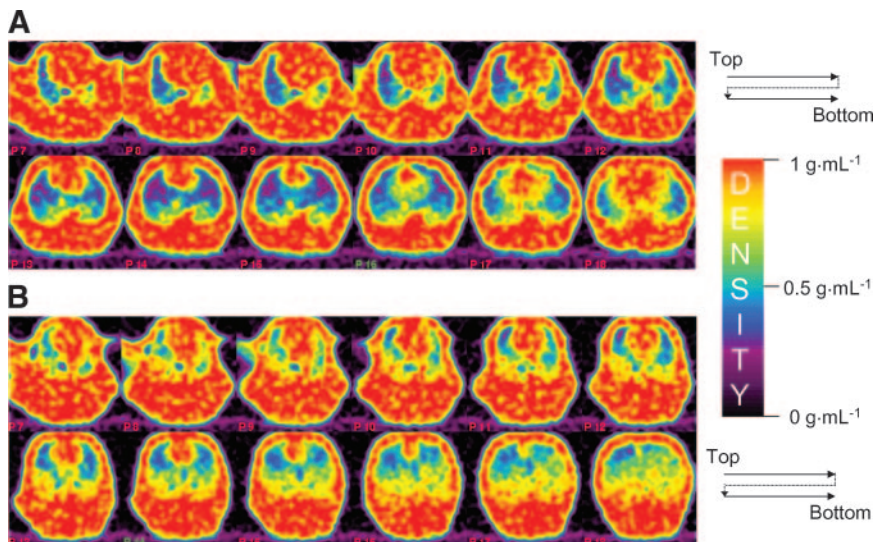


FIGURE 3. Parametric images of thorax density obtained in control pig (A) and in pig with lung injury (B). Slices are displayed according to radiologic convention. In each pig, only 12 of 19 planes are displayed for clarity.

tion in pulmonary veins, and $CPA(t)$ is $^{13}\text{N-N}_2$ concentration in pulmonary artery.

Assuming full tracer equilibration between alveolar gas and end-capillary blood, $C_V(t)$ can be approximated by the product of $CA(t)$ times the nitrogen gas–water partition coefficient ($\lambda_{\text{N}_2 \text{ water/air}}$), which equals to 0.019 (19). In this condition, $C_V(t)$ and $CPA(t)$ are assumed to be negligible (20). Moreover, if tracer regional re-breathing is neglected during $^{13}\text{N-N}_2$ washout, $C(t)$ is approximated to zero and Equation 2 can be rewritten as:

$$\frac{dCA(t)}{dt} = \frac{-\dot{V}_A}{V_A} \times CA(t). \quad \text{Eq. 3}$$

Given that PET is unable to (a) separate radioactivity originating from the blood, lung parenchyma, or alveolar spaces and (b) produce instantaneous measurement of tracer concentration, each PET image represents the sum of all radioactivity events occurring during acquisition time. Then, for each frame i collected between t_i and $t_i + \Delta t_{\text{img}}(i)$:

$$CPET(i) = \frac{\int_{t_i}^{t_i + \Delta t_{\text{img}}(i)} (CA(t)V_A + CLP(t)V_{LP} + CB(t)V_B) dt}{V_{ROI}}, \quad \text{Eq. 4}$$

where $i = 1, 2, 3, \dots$, is total number of frames; $CPET(i)$ is tracer concentration in lung ROI assessed with PET in frame i ; $CLP(t)$ and $CB(t)$ are tracer concentration within the lung parenchyma and blood, respectively; V_{LP} , V_B , and V_{ROI} are lung parenchyma, blood, and ROI volume, respectively; and $\Delta t_{\text{img}}(i)$ is duration of acquisition of frame i .

As stated above, nitrogen diffusion in tissue is assumed as negligible, then:

$$CPET(i) = \frac{\int_{t_i}^{t_i + \Delta t_{\text{img}}(i)} V_A \cdot CA(t) dt}{V_{ROI}}. \quad \text{Eq. 5}$$

Equations 3 and 5 are operational equations required to solve this monocompartmental model for V_A and \dot{V}_A/V_A . \dot{V}_A was then computed by multiplying V_A by \dot{V}_A/V_A .

Bicompartmental Model. Assuming 2 alveolar compartments, tracer kinetics can be described by the following system of differential equations:

$$\begin{aligned} \frac{dCA_1(t)}{dt} &= \frac{-\dot{V}_{A_1}}{V_{A_1}} \times CA_1(t), \\ \frac{dCA_2(t)}{dt} &= \frac{-\dot{V}_{A_2}}{V_{A_2}} \times CA_2(t), \end{aligned} \quad \text{Eq. 6}$$

with indices 1 and 2 indicating fast and slow compartments, respectively.

Solving Equation 6 for CA_1 , CA_2 , V_{A_1} , and V_{A_2} gives CA_{1+2} ($^{13}\text{N-N}_2$ alveolar concentration in compartment 1+2) with:

$$CA_{1+2} = \frac{CA_1 \times V_{A_1} + CA_2 \times V_{A_2}}{(V_{A_1} + V_{A_2})}. \quad \text{Eq. 7}$$

Finally, inserting CA_{1+2} in Equation 5 gives:

$$CPET(i) = \frac{\int_{t_i}^{t_i + \Delta t_{\text{img}}(i)} (V_{A_1} + V_{A_2}) \cdot CA_{1+2}(t) dt}{V_{ROI}}. \quad \text{Eq. 8}$$

Equations 6 and 8 are operational equations required to solve this bicompartmental model for V_{A_1} , V_{A_2} , \dot{V}_{A_1}/V_{A_1} , and \dot{V}_{A_2}/V_{A_2} . \dot{V}_{A_1}

and \dot{V}_{A_2} were then computed by multiplying V_{A_1} by \dot{V}_{A_1}/V_{A_1} and V_{A_2} by \dot{V}_{A_2}/V_{A_2} , respectively.

Finally, alveolar gas volume and ventilation were calculated as follows:

$$\begin{aligned} V_A &= V_{A_1+2} = V_{A_1} + V_{A_2}, \\ \dot{V}_A &= \dot{V}_{A_1+2} = \frac{\dot{V}_{A_1} \times V_{A_1} + \dot{V}_{A_2} \times V_{A_2}}{V_{A_1} + V_{A_2}}. \end{aligned} \quad \text{Eq. 9}$$

Parameter Identification. Nonlinear regression was used to find out model parameters $V_{A_{\text{emission}}}$ and $\dot{V}_{A_{\text{emission}}}$. The Levenberg–Marquardt algorithm was used to minimize the sum of squared errors between model output and experimental data. Differential equations were solved using Matlab (The Mathworks) “ode45” solver for nonstiff differential equations, with initial value for CA at $t = 0$ set to C_{INPUT} . Numeric integration was performed using the trapezoid method.

Model Selection. In each ROI, the best model was selected using residual analysis as an estimate of the goodness of fit (21) and extra sum of square analysis for nested models (22).

Statistical Analysis

Unless otherwise stated, data are presented as median and interquartile range [IQR]. Linear regression analyses were performed by the least-squares method and correlations assessed with the Pearson correlation coefficient. Comparisons between control and OA groups were made using the Mann–Whitney rank sum test. Comparisons between pigs were performed using the Kruskal–Wallis test with the Tukey test for post hoc pairwise comparisons among subgroups. Bias (23) was compared with zero using a 1-sample t test. Statistical analysis were performed using SPSS for Windows (SPSS Inc.), and the level of statistical significance was set at $P < 0.05$.

RESULTS

PET images of a control pig and an OA-injured pig are displayed on Figures 3 and 4. Lung density was markedly increased in the injured pig (0.72 [0.64–0.78] g/mL) compared with the control pig (0.59 [0.53–0.67] g/mL), particularly in dorsal regions where pulmonary edema is prominent (Fig. 3). Similarly, on emission scans, $^{13}\text{N-N}_2$ activity in dependent regions is clearly lower in the injured pig than in the control pig (Fig. 4).

Regional PET measurements were made in a total of 749 ROIs (38 [37–38] per experimental condition per pig) and, hence, mathematic modeling was performed in each of the 749 time–activity curves generated by image analysis. As shown on Figure 5A, the monocompartmental model underestimated lung activity assessed with PET, especially after the first minute of washout. This was confirmed by a residual distribution skewed below zero (Fig. 5B). In contrast, the bicompartmental model adequately fitted experimental data points during washout (Fig. 5C), as shown by a random distribution of residuals around 0 (Fig. 5D). As can be seen in Figure 5E, the superiority of the bicompartmental model over the monocompartmental model in this particular ROI is clearly demonstrated. Furthermore, for the whole dataset, the extra sum of square analysis showed that the

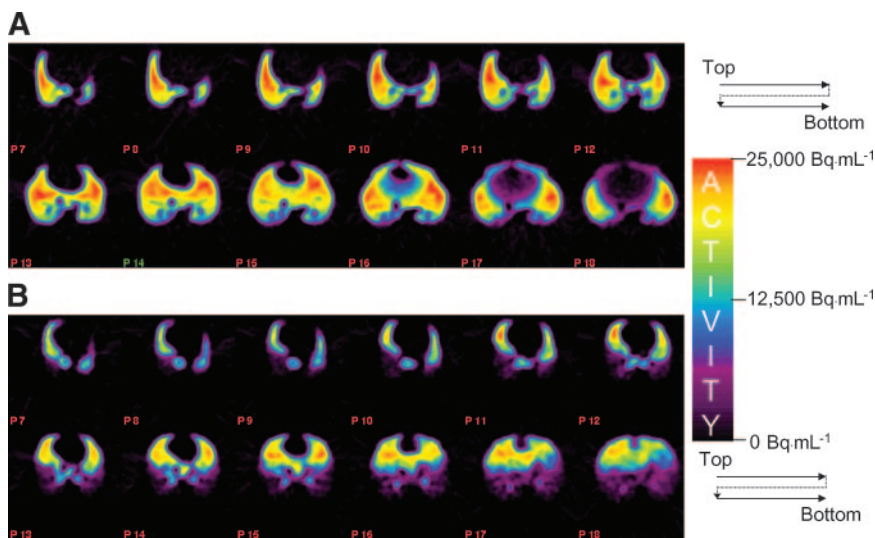


FIGURE 4. First frame of $^{13}\text{N-N}_2$ washout obtained in control pig (A) and in pig with lung injury (B). Slices are displayed according to radiologic convention. In each pig, only 12 of 19 planes are displayed for clarity.

bicompartmental model was selected over the monocompartmental model in 94.7% [62.2%–100.0%] of the ROIs in the control group and in 90.7% [81.6%–97.4%] in the OA group ($P = 0.49$ between control and OA groups).

The contribution of fast and slow compartments (i.e., compartment with highest and lowest \dot{V}_A , respectively) differed between control and injured animals. The fast compartment amounted to 94.4% [93.4%–95.5%] and 95.6% [94.3%–99.5%] of total alveolar gas volume in control pigs 1 and 2, respectively, and to 79.9% [79.6%–83.4%] and 82.7% [81.0%–83.9%] in injured pigs 1 and 2, respectively ($P = 0.003$ vs. control pig 1 and 2).

The validity of the estimates of $V_{A\text{emission}}$ and $\dot{V}_{A\text{emission}}$ provided by the best model fitting was tested in 2 different ways. First, a strong linear relationship was found between regional alveolar gas volume obtained from $^{13}\text{N-N}_2$ washout ($V_{A\text{emission}}$) on one hand and from lung density analysis of the transmission scan ($V_{A\text{trans}}$) on the other hand (Fig. 6A) in all 749 ROIs. However, estimates of $V_{A\text{emission}}$ were slightly but significantly overestimated (Fig. 6B) compared with $V_{A\text{trans}}$ (mean $V_{A\text{emission}} - V_{A\text{trans}} = 0.96$, $P < 0.001$ by comparison with zero). It should be noted, however, that only 5% of the experimental points were beyond the 95% confidence interval of the limits of agreement (Fig. 6B). Second, the positive correlations between $\dot{V}_{A\text{emission}}$ (Fig. 7A) or $\dot{V}_{A\text{emission}}/V_{A\text{emission}}$ (Fig. 7B) and \dot{V}_E were highly statistically significant in both control and OA groups.

DISCUSSION

In this study, we describe a new mathematic model to quantify regional lung ventilation during $^{13}\text{N-N}_2$ washout using PET. The main findings of this study were that (a) the developed mathematic model provided an accurate description of pulmonary $^{13}\text{N-N}_2$ kinetics, (b) $^{13}\text{N-N}_2$ kinetics were best described by a bicompartmental model, especially in injured lungs, (c) PET of regional $^{13}\text{N-N}_2$ washout accu-

rately measured the alveolar gas volume, and (d) estimates of \dot{V}_A correlated well with \dot{V}_E as the independent variable.

Comparison with Alternate Methods for Quantifying Lung Ventilation with PET

The present method presents several advantages over previously described methods using PET. Unlike previous studies requiring specific ventilators with closed circuits (9,24), the present method uses an open circuit to administer $^{13}\text{N-N}_2$ and then can be easily applied to any intensive care unit ventilator. Intravenous injection of $^{13}\text{N-N}_2$ is an alternate method to assess alveolar ventilation with PET (10,25,26), but it cannot be considered as an ideal method for several reasons. First, ventilation cannot be determined in areas with low or no perfusion (9). Although measuring ventilation in these regions may be of little importance in explaining arterial oxygenation, ventilation and volume assessment in all lung regions are required to fully investigate some conditions such as VILI. Second, this method requires an apneic period of 40–60 s after tracer bolus injection, potentially resulting in alveolar derecruitment, especially if performed on zero end-expiratory pressure. Finally, this prolonged apnea may be poorly tolerated in animals during experimental lung injury and precludes application of this technique in ALI patients.

Methodologic Issues

As a prerequisite for modeling accuracy, unbiased quantitation of lung radioactivity is required. With PET, and especially in the lungs, radioactivity measurement is hindered by the partial-volume effect related to ventilation-induced thoracic movements. Respiratory gating or respiratory motion tracking options coupled with list-mode acquisition of both transmission and emission data are attractive methods to minimize quantitation problems but are not available for dynamic studies with our PET camera. Moreover, gating-related improvement in image quality is balanced with dramatic diminution in counting statistics,

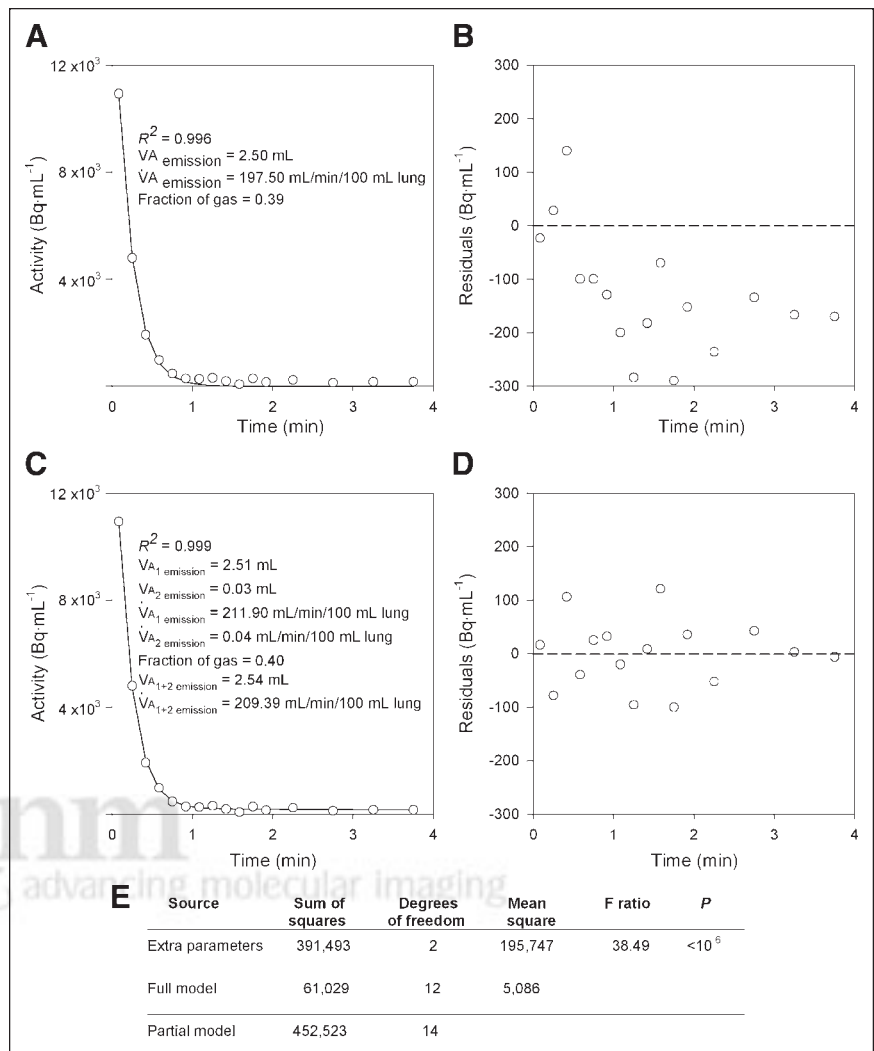


FIGURE 5. Examples of curve fitting using monocompartmental model (A) and bicompartmental model (C) for the same representative ROI in a control pig. \circ , Time-activity curve data points obtained with PET. Continuous lines are fitted data using monocompartmental or bicompartmental model. (B) and (D) Corresponding plots of residuals over time. (E) Extra sum of square analysis for nested models as a way to compare relevance of models.

making this method unsuitable for dynamic studies requiring high temporal sampling. We can speculate that the partial-volume effect should primarily affect quantitation of peripheral anterior regions that exhibit the greatest move-

ments in supine position, thus being responsible for an increase in time-activity curve experimental "noise" and a decrease in model parameter estimation accuracy. Additionally, spillover from radioactivity originating from extrapul-

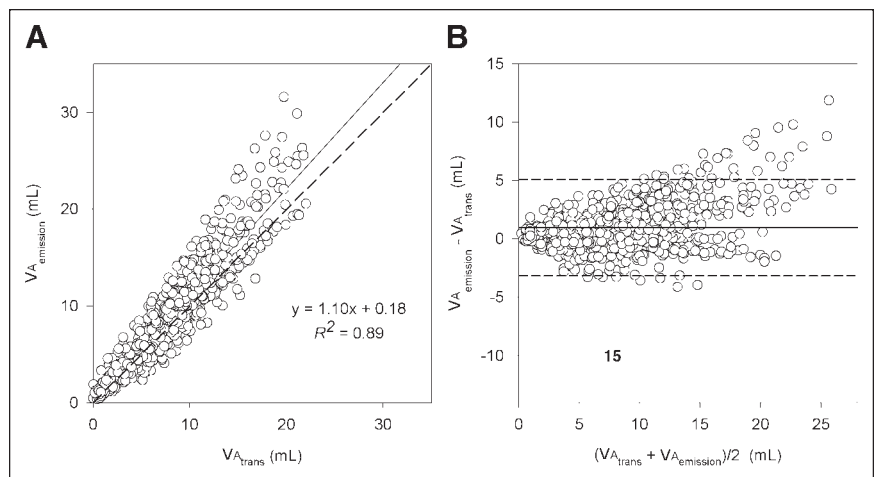


FIGURE 6. (A) Relationship between regional alveolar gas volume measured from transmission ($V_{A \text{ trans}}$) and emission scans ($V_{A \text{ emission}}$). Each symbol is the regional value of V_A in one lung ROI in a given experimental condition in 1 animal. The total number of ROIs amounts to 749. Solid and dashed lines are regression line and line of identity, respectively. (B) Bland-Altman representation (23) of relationship shown in A. Solid and dashed lines represent mean and mean \pm SD, respectively.

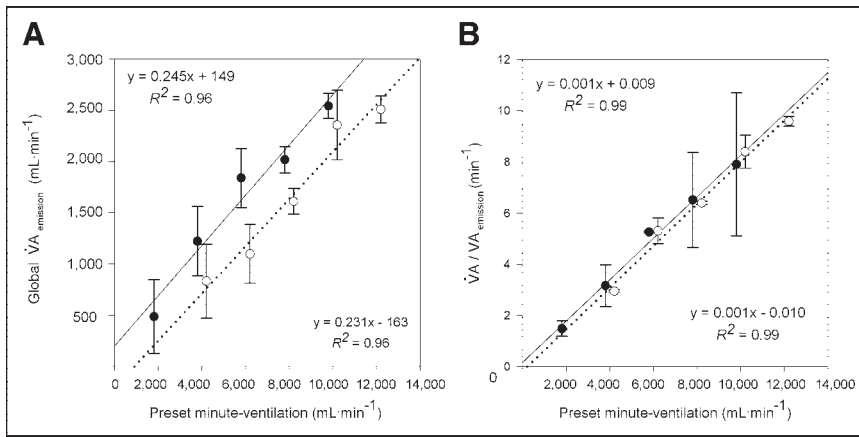


FIGURE 7. Relationships between preset minute-ventilation and alveolar ventilation ($V_{A\text{émission}}$, A) or specific ventilation ($\dot{V}_A/V_{A\text{émission}}$, B) assessed with PET in control pigs (●) and pigs with lung injury (○). For each pig, $V_{A\text{émission}}$ and $\dot{V}_A/V_{A\text{émission}}$ were measured regionally using modeling in each ROI. Regional values of $V_{A\text{émission}}$ were summed to obtain global ventilation expressed as mean \pm SD for each experimental group (A). Median values of regional $\dot{V}_A/V_{A\text{émission}}$ were calculated for each animal and data were finally expressed as mean \pm SD for each experimental group (B). Bars are SDs. Solid and dotted lines are regression lines for control and oleic acid groups, respectively.

ues of regional $\dot{V}_A/V_{A\text{émission}}$ were calculated for each animal and data were finally expressed as mean \pm SD for each experimental group (B). Bars are SDs. Solid and dotted lines are regression lines for control and oleic acid groups, respectively.

monary regions is not expected to generate much problem of lung radioactivity quantitation in this study because blood diffusion of $^{13}\text{N-N}_2$ is assumed to be negligible.

However, accurate measurement of lung radioactivity requires accurate ROI determination. In pulmonary PET studies, the transmission scan is generally used to delineate lung boundaries (16,26,27). Because pulmonary edema predominates in dependent regions during ALI, these regions may be wrongly excluded during the ROI determination process (Fig. 3). Using the emission scan to delineate these regions is not an option when dealing with inhaled radioactive tracers because low or nonventilated areas receive little to no radioactivity and cannot be identified (Fig. 4). To overcome this problem, H_2^{15}O equilibrium images were used (17) to refine ROI boundaries in dependent regions, easily seen because of their high water content.

Assuming accurate determination of time-activity curves with PET, the accuracy of physiologic parameters assessed from mathematic models greatly depends on assumptions required to build the model, and extensive discussion of their validity is required. First, the present model assumes negligibility of tracer removal by pulmonary blood, based on the low value of $\lambda_{\text{N}_2\text{ water/air}}$ (19). This was verified by the lack of radioactivity within ROIs drawn on cardiac regions. Second, tracer equilibration within alveolar gas is required to obtain valid measurement of alveolar gas volume. This assumption was regionally verified in preliminary experiments in both control and injured pigs, where regional equilibrium during $^{13}\text{N-N}_2$ inhalation was always obtained within 4 min. Third, as in previous washout studies with PET (20), the effect of anatomic dead-space ventilation on the $^{13}\text{N-N}_2$ mass equation in alveolar spaces was assumed to be negligible. This simplification is expected to induce an underestimation of \dot{V}_A , the extent of which is dependent on the anatomic dead space of the region. This partly explains the slope of the relationship between preset \dot{V}_E and \dot{V}_A assessed with PET.

Model Validity

Model validity was first demonstrated by adequate fitting of time-activity curves using the bicompartamental model, suggesting ventilation heterogeneity within ROIs in both normal and injured pigs. This result is not surprising, given the relatively large size of the ROIs drawn in this study (21.0 [12.3–31.7] mL) and that the corresponding time-activity curves represent tracer clearance from multiple regions within an isogravitational plane. Using a bicompartamental model is certainly an oversimplification of a system that has spatial heterogeneity at length scale much smaller than the spatial resolution of PET (28). However, increasing the number of compartments of the model would not increase the accuracy of regional ventilation assessment because experimental error in radioactivity measurements precludes acquisition of noise-free curves required for multicompartamental modeling. Nevertheless, the ability of the bicompartamental model to tightly fit experimental data points confirms that this model is able to estimate an average regional behavior of ventilation within the ROIs. Furthermore, our results are in accordance with a previous study using dynamic CT in lung lavage-induced ALI (29). Using biexponential fitting of the aerated lung, the fast compartment represented 86% of the lung volume that became aerated by increasing airway pressure from zero end-expiratory pressure, whereas the slow compartment accounted for 14% (29). These findings are additional evidence for the validity of our modeling approach.

Second, regional validation of $V_{A\text{émission}}$ was performed using density analysis on the transmission scan. Despite a close correlation between both measurements, $^{13}\text{N-N}_2$ kinetics modeling slightly overestimates the lung volume (by approximately 10%), as reflected by the slope of the regression line (1.1) between $V_{A\text{émission}}$ and $V_{A\text{trans}}$ (Fig. 6A). However, this difference may be fully explained by an error in density determination in vivo by PET. Indeed, due to the reconstruction procedure of the transmission scan, values of

density within regions surrounded by structures of high density (such as thoracic wall or mediastinum) are overestimated. From phantom studies, this overestimation of pulmonary density amounts to 0.026 g/mL (30). Assuming a similar value in our study, this error explains a density overestimation of approximately 8% and then an underestimation in $V_{A_{trans}}$ of similar magnitude.

Third, regional values of $\dot{V}_{A_{emission}}$ were added up to obtain a global estimation of \dot{V}_A with PET, which correlated well with \dot{V}_E , despite an apparent systematic underestimation as shown by regression lines slopes below 0.25 in both normal and injured pigs (Fig. 7A). This may be explained by 3 facts. (i) Image analysis excluded the extreme top and bottom parts of the lungs because of the limited longitudinal field of view (15.4 cm) of the PET camera. Thus, probably only 80% of the lung was included in the determination of $\dot{V}_{A_{emission}}$ in our study. (ii) Preset \dot{V}_E includes anatomic dead-space ventilation and, hence, overestimates global alveolar ventilation by approximately 30%, assuming a volume of dead space/tidal volume (V_{DS}/V_T) value of this magnitude. (iii) $^{13}\text{N-N}_2$ rebreathing has been considered as negligible during modeling, and this simplification may underestimate regional \dot{V}_A , depending on regional V_{DS}/V_T variability. Interestingly, normal and injured lungs apparently behaved in the same way as shown by similar regression lines (Fig. 7), suggesting no significant effect of lung injury on regional V_{DS}/V_T and modeling validity.

Practical Implications

The present method allows a systematic description of regional alveolar volume and ventilation, which can be applied directly in mechanically ventilated intensive care unit patients, provided transport to a PET facility is compatible with the patient's condition. Alveolar overdistension may be derived from the regional fraction of gas to better understand the pathophysiologic mechanisms of VILI. However, application in patients may be hindered by the limited longitudinal field of view of current-generation PET scanners, requiring at least 2 bed positions to study the entire lung, therefore increasing both radiation burden and costs.

The recent availability of combined PET/CT scanners has the potential to further refine the present technique, allowing reduced acquisition time with increased spatial resolution, better ROI boundary delineation, and assessment of alveolar gas volume based on a CT-derived density map. To date, however, multiframe acquisition of tracer kinetics within the lung with PET/CT scanners remains challenging and would require sophisticated hardware and data-processing algorithms to correct static CT images and respiratory-averaged PET emission data for respiratory and cardiac motions. Respiratory gating or respiratory motion tracking options coupled with list-mode acquisition during attenuation and emission are possible solutions to this problem but remain to be developed for commercial PET/CT machines.

Finally, additional work in other animal models of ALI are required before the reliability of the present method can be verified in patients with ALI or adult respiratory distress syndrome.

CONCLUSION

We have provided a simple and accurate method to quantify regional lung volume and alveolar ventilation using inhaled $^{13}\text{N-N}_2$ and PET. Taking into account regional heterogeneity in alveolar ventilation, a bicompartmental model described $^{13}\text{N-N}_2$ lung kinetics better than a mono-compartmental model. This method can now be systematically used to investigate how the distribution of lung ventilation can be changed by interventions, such as positive end-expiratory pressure, prone position, or recruitment maneuvers, and how these changes may affect VILI.

APPENDIX

- C_A = alveolar concentration of $^{13}\text{N-N}_2$
- C_{INPUT} = inhaled tracer concentration at equilibrium
- $\lambda_{N_2 \text{ water/air}}$ = nitrogen gas-water partition coefficient
- V_A = alveolar gas volume
- $V_{A_{trans}}$ = alveolar gas volume assessed on transmission scans
- $V_{A_{emission}}$ = alveolar gas volume assessed on emission scans
- \dot{V}_A = alveolar ventilation
- $\dot{V}_{A_{emission}}$ = alveolar ventilation assessed on emission scans
- \dot{V}_E = minute ventilation
- V_T = tidal volume

ACKNOWLEDGMENTS

The authors thank Fabienne Bregeon and Gael Bourdin for their help with animal preparation. This study was supported by grants from Hospices civils de Lyon, Equipe d'accueil 1896 and Claude Bernard Lyon I University (Bonus Qualité Recherche).

REFERENCES

1. Dreyfuss D, Saumon G. Ventilator-induced lung injury: lessons from experimental studies. *Am J Respir Crit Care Med.* 1998;157:294-323.
2. Muscedere JG, Mullen JB, Gan K, Slutsky AS. Tidal ventilation at low airway pressures can augment lung injury. *Am J Respir Crit Care Med.* 1994;149:1327-1334.
3. The Acute Respiratory Distress Syndrome Network. Ventilation with lower tidal volumes as compared with traditional tidal volumes for acute lung injury and the acute respiratory distress syndrome. *N Engl J Med.* 2000;342:1301-1308.
4. Petersson J, Sanchez-Crespo A, Rohdin M, et al. Physiological evaluation of a new quantitative SPECT method measuring regional ventilation and perfusion. *J Appl Physiol.* 2004;96:1127-1136.
5. Marcucci C, Nyhan D, Simon BA. Distribution of pulmonary ventilation using Xe-enhanced computed tomography in prone and supine dogs. *J Appl Physiol.* 2001;90:421-430.
6. Deninger AJ, Mansson S, Petersson JS, et al. Quantitative measurement of regional lung ventilation using ^3He MRI. *Magn Reson Med.* 2002;48:223-232.
7. Porra L, Monfraix S, Berruyer G, et al. Effect of tidal volume on distribution of ventilation assessed by synchrotron radiation CT in rabbit. *J Appl Physiol.* 2004;96:1899-1908.
8. Rhodes CG, Valind SO, Brudin LH, Wollmer PE, Jones T, Hughes JM. Quantification of regional V/Q ratios in humans by use of PET. I. Theory. *J Appl Physiol.* 1989;66:1896-1904.

9. Vidal Melo MF, Layfield D, Harris RS, et al. Quantification of regional ventilation-perfusion ratios with PET. *J Nucl Med.* 2003;44:1982-1991.
10. O'Neill K, Venegas JG, Richter T, et al. Modeling kinetics of infused ^{13}N -saline in acute lung injury. *J Appl Physiol.* 2003;95:2471-2484.
11. Venegas JG, Tsuzaki K, Fox BJ, Simon BA, Hales CA. Regional coupling between chest wall and lung expansion during HFV: a positron imaging study. *J Appl Physiol.* 1993;74:2242-2252.
12. Grotjohan HP, van der Heijde RM, Jansen JR, Wagenvoort CA, Versprille A. A stable model of respiratory distress by small injections of oleic acid in pigs. *Intensive Care Med.* 1996;22:336-344.
13. Schuster DP. ARDS: clinical lessons from the oleic acid model of acute lung injury. *Am J Respir Crit Care Med.* 1994;149:245-260.
14. Le Bars D. A convenient production of [^{13}N] nitrogen for ventilation studies using a nitrogen gas target for ^{13}C production. *J Labelled Compds Radiopharm.* 2001;44:1-5.
15. Brix G, Zaers J, Adam LE, et al. Performance evaluation of a whole-body PET scanner using the NEMA protocol: National Electrical Manufacturers Association. *J Nucl Med.* 1997;38:1614-1623.
16. Richard JC, Janier M, Lavenne F, et al. Effect of position, nitric oxide, and almitrine on lung perfusion in a porcine model of acute lung injury. *J Appl Physiol.* 2002;93:2181-2191.
17. Chen DL, Schuster DP. Positron emission tomography with [^{18}F]fluorodeoxyglucose to evaluate neutrophil kinetics during acute lung injury. *Am J Physiol Lung Cell Mol Physiol.* 2004;286:L834-L840.
18. Schuster DP, Marklin GF, Mintun MA, Ter-Pogossian MM. PET measurement of regional lung density: 1. *J Comput Assist Tomogr.* 1986;10:723-729.
19. Rosenthal MS, Nickles RJ. Selected noble-gas partition coefficients. *Phys Med Biol.* 1985;30:945-950.
20. Galletti GG, Venegas JG. Tracer kinetic model of regional pulmonary function using positron emission tomography. *J Appl Physiol.* 2002;93:1104-1114.
21. Carson RE. Parameter estimation in positron emission tomography. In: Phelps ME, Mazziotta J, Schelbert HR, eds. *Positron Emission Tomography and Autoradiography: Principles and Applications for the Brain and Heart.* New York, NY: Raven Press; 1986:347-390.
22. Bates DM, Watts DG. Practical considerations in nonlinear regression. In: *Nonlinear Regression Analysis and its Applications.* New York, NY: John Wiley & Sons, Inc.; 1988:67-133.
23. Bland JM, Altman DG. Statistical methods for assessing agreement between two methods of clinical measurement. *Lancet.* 1986;1:307-310.
24. Treppo S, Mijailovich SM, Venegas JG. Contributions of pulmonary perfusion and ventilation to heterogeneity in V_A/Q measured by PET. *J Appl Physiol.* 1997;82:1163-1176.
25. Willey-Courand DB, Harris RS, Galletti GG, Hales CA, Fischman A, Venegas JG. Alterations in regional ventilation, perfusion, and shunt after smoke inhalation measured by PET. *J Appl Physiol.* 2002;93:1115-1122.
26. Musch G, Harris RS, Vidal Melo MF, et al. Mechanism by which a sustained inflation can worsen oxygenation in acute lung injury. *Anesthesiology.* 2004;100:323-330.
27. Schuster DP, Sandiford P, Stephenson AH. Thromboxane receptor stimulation/inhibition and perfusion redistribution after acute lung injury. *J Appl Physiol.* 1993;75:2069-2078.
28. Altemeier WA, McKinney S, Glenny RW. Fractal nature of regional ventilation distribution. *J Appl Physiol.* 2000;88:1551-1557.
29. Markstaller K, Eberle B, Kauczor HU, et al. Temporal dynamics of lung aeration determined by dynamic CT in a porcine model of ARDS. *Br J Anaesth.* 2001;87:459-468.
30. Brudin LH, Rhodes CG, Valind SO, Wollmer P, Hughes JM. Regional lung density and blood volume in nonsmoking and smoking subjects measured by PET. *J Appl Physiol.* 1987;63:1324-1334.

